Physics Letters A 374 (2010) 4014–4017

Contents lists available at ScienceDirect

Physics Letters A

www.elsevier.com/locate/pla

Phase characterization of experimental gas–liquid two-phase flows

Zhong-Ke Gao [a,b,*], Ning-De Jin [a], Wen-Xu Wang [b], Ying-Cheng Lai [b,c]

[a] School of Electrical Engineering and Automation, Tianjin University, Tianjin 300072, China
[b] School of Electrical, Computer and Energy Engineering, Arizona State University, Tempe, AZ 85287, USA
[c] Department of Physics, Arizona State University, Tempe, AZ 85287, USA

ARTICLE INFO

Article history:
Received 4 June 2010
Received in revised form 4 August 2010
Accepted 4 August 2010
Available online 7 August 2010
Communicated by C.R. Doering

Keywords:
Nonlinear time series analysis
Two-phase flow
Phase characterization
Nonlinear systems

ABSTRACT

We propose a method to characterize and distinguish flow patterns in experimental two-phase (e.g., gas–liquid) flows. The basic idea is to calculate the instantaneous phase from the signal and to extract scaling behaviors associated with the phase fluctuations. The effectiveness of the method is demonstrated and its applicability is articulated.

Gas–liquid two-phase flows arise commonly in a variety of physical, engineering, and industrial applications such as filtration, lubrication, spray processes, natural gas networks, and nuclear reactor cooling, etc. Understanding the nonlinear and complex dynamics underlying gas–liquid flows is a significant but challenging problem. In this regard, a primary task is to characterize and quantify the various flow patterns that often appear complex. Generally, the patterns arising from two-phase flows depend on a number of factors including the type of gas–liquid combination, the flow rate and direction, the shape, size, and inclination of the conduit. A common practice in the field is to examine the fluctuating properties associated with two-phase flows, which can be experimentally assessed from measurements such as the local pressure and the instantaneous two-phase mixture ratio [1,2]. Existing methods aiming at characterizing the fluctuations include those based on the power-spectral density (PSD) for pressure drop [3] and transient x-ray attenuation techniques [4,5]. Standard time-series analysis methods from nonlinear dynamics and chaos [6] have also been exploited [7–10].

At the present, the dynamical mechanisms generating various patterns in gas–liquid two-phase flows are elusive, due to the complex and nonlinear interplay among many factors such as fluid turbulence, phase interfacial interaction, and local relative movement between phases, etc. To our knowledge, a systematic theoretical framework to predict the flow patterns is non-existent. The purpose of this Letter is to introduce a instantaneous-phase based method to characterize typical patterns from experimental gas–liquid flows. Our idea is that the phase fluctuations associated with time series are caused by the intrinsic dynamics and can therefore yield important information about the underlying flow that existing, non-phase based methods are incapable of revealing. In particular, given a set of experimentally measured conductance-fluctuating signals, we first use the empirical-mode decomposition (EMD) method pioneered by Huang et al. [11] to extract the phase fluctuations. To uncover any robust scaling behavior hidden in the phase fluctuations, we use detrended fluctuation analysis (DFA) [12]. Our main finding is that, for each of the three distinct patterns arising typically in experimental two-phase flows, a scaling exponent can be extrapolated from the phase fluctuations. For different flow patterns, the values of the exponent are statistically distinct, indicating the effectiveness of the combined EMD/DFA method to characterize and distinguish complex two-phase flow patterns.

Our data are conductance signals from vertically upward pipe of inner diameter 125 mm in multi-phase flow-loop experiments at Tianjin University. The experimental mediums are air and tap water. The experimental system consists of the pipe, a vertical multi-electrode array (VMEA) of conductance sensors [13], high-speed video camera recorder (VCR), exciting-signal generating circuit, signal modulating module, data-acquisition device (PXI 4472, National Instruments), and software for preliminary signal processing. The VMEA component is shown in Fig. 1. The measurement system

* Corresponding author.
E-mail address: zhongkegao@tju.edu.cn (Z.-K. Gao).

0375-9601/$ – see front matter
doi:10.1016/j.physleta.2010.08.005

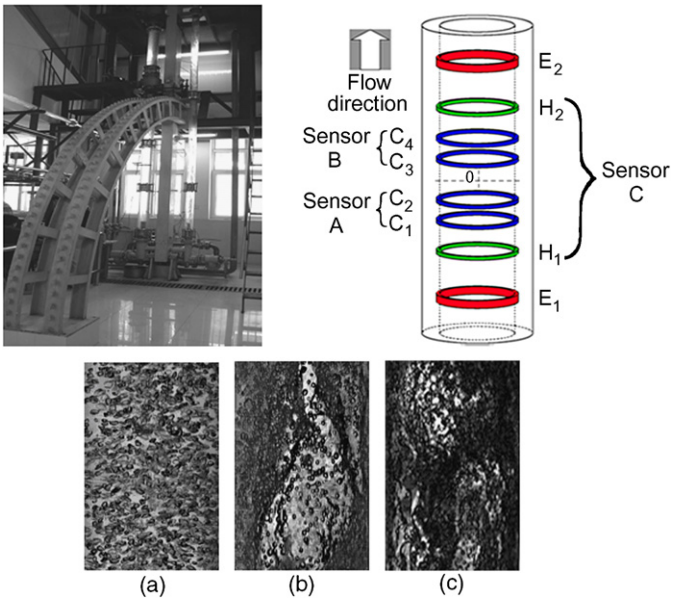

Fig. 1. (Color online.) VEMA sensor and three typical patterns experimentally recorded from vertically upward gas–liquid two-phase flows: (a) bubble flow ($U_{sw} = 0.18$ m/s, $U_{sg} = 0.01$ m/s), (b) slug flow ($U_{sw} = 0.18$ m/s, $U_{sg} = 0.12$ m/s), and (c) churn flow ($U_{sw} = 0.18$ m/s, $U_{sg} = 0.61$ m/s). The VEMA consists of eight alloy titanium ring electrodes axially separated and flush mounted on the inside wall of the flowing pipe. E1 and E2 are exciting electrodes. C1–C2 and C3–C4 are two pairs of upstream and downstream correlation electrodes denoted as sensor A and sensor B, respectively. Based on the cross-correlation technique, we can extract the axial velocity of the two-phase flow from fluctuating signals from sensors A and B. H1–H2 is the volume-fraction electrodes denoted as sensor C. The measurement circuit is embedded inside the instrument.

uses a 20 kHz sinusoidal voltage signal of amplitude 1.4 V to excite the flow. The signal-modulating module consists of three submodules: differential amplifier, sensitive demodulation and low-pass filter.

A typical experimental run starts by generating water flow at a fixed rate in the pipe and then gradually increasing the gas-flow rate. When the gas and water flow rates reaches a pre-defined ratio, a conductance signal is collected from VMEA and the flow pattern is visualized by the high-speed VCR. Fig. 1 shows three typical patterns from the water–gas flows. The water- and gas-flow rates are between 0.02 m/s and 0.27 m/s and from 0.0045 m/s to 2.94 m/s, respectively. The sampling frequency is 400 Hz, and the data recording time for one measurement point is 60 s.

Let $b(t)$ be a measured conductance-fluctuating signal. To see the need for the EMD method, we first perform the Hilbert transform:

$$b'(t) = P.V.\left[1/\pi \int_{-\infty}^{+\infty} b(t')/(t-t')\,dt'\right] \tag{1}$$

where $P.V.$ stands for the Cauchy principal value for integral. We then construct the corresponding analytic signal as

$$\psi(t) = b(t) + ib'(t) \tag{2}$$

Fig. 2(a) shows, for a signal from the bubble flow, a trajectory of the analytic signal in its complex plane. We observe that there exist multiple centers of rotation, so a properly defined phase variable cannot be obtained from the analytic signal. It is thus necessary to decompose the original signal $b(t)$ into a number of modes whose analytic signals correspond to proper rotations. Similar behaviors have been observed for slug and churn flows.

The EMD method was invented [11] to address this decomposition problem. The method has been applied to different problems

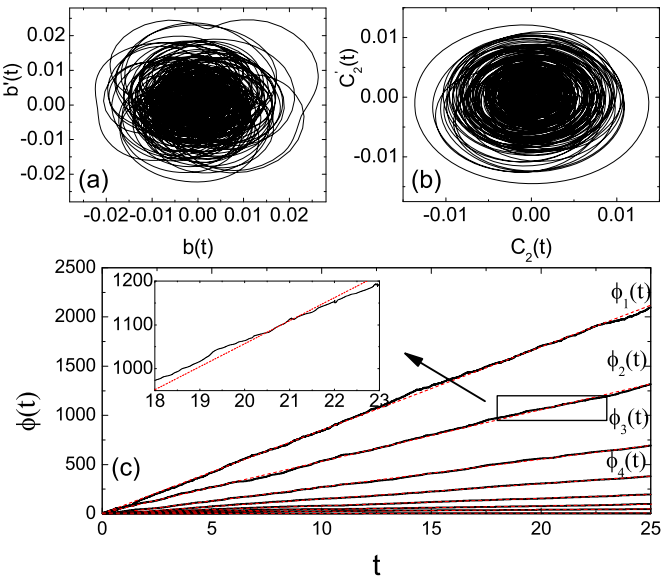

Fig. 2. (Color online.) Trajectory in the complex plane of the analytic signal from a bubble flow ($U_{sw} = 0.18$ m/s, $U_{sg} = 0.01$ m/s): (a) for the original signal and (b) for the second intrinsic mode. (c) Phase function $\phi_k(t)$ corresponding to eight different intrinsic modes from the bubble flow. The red dashed lines are the linear fitting of phase functions. The extracted frequencies of these modes are $w_1 \approx 84.66$, $w_2 \approx 52.54$, $w_3 \approx 28.26$, $w_4 \approx 15.47$, $w_5 \approx 7.6$, $w_6 \approx 3.5$, $w_7 \approx 1.7$, and $w_8 \approx 0.29$.

such as phase characterization of chaos [14] and laser signals [15]. The basic steps of the EMD method are: (1) construction of two smooth splines connecting all the maxima and minima, respectively, to get $b_{max}(t)$ and $b_{min}(t)$; (2) computation of

$$\Delta b(t) \equiv b(t) - \left[b_{max}(t) + b_{min}(t)\right]/2 \tag{3}$$

and (3) repetitions of steps (1) and (2) for $\Delta b(t)$ until the resulting signal corresponds to a proper rotation. Denote the resulting signal by $C_1(t)$, which is the first intrinsic mode. We then take the difference

$$b_1(t) \equiv b(t) - C_1(t) \tag{4}$$

and repeat steps (1)–(3) to obtain the second intrinsic mode $C_2(t)$. The procedure continues until the mode $C_M(t)$ shows no apparent variation (i.e., it has fewer than two local extrema). Result from the decomposition procedure can thus be represented by

$$b(t) = \sum_{k=1}^{M} C_k(t) \tag{5}$$

where the intrinsic modes $C_k(t)$ are nearly orthogonal to each other [11]. By construction, each mode $C_k(t)$ generates a proper rotation in the complex plane of its own analytic signal

$$\psi_k(t) = A_k(t)e^{i\phi_k(t)} \tag{6}$$

and the average rotation frequencies

$$w_k = \left\langle d\phi_k(t)/dt \right\rangle \tag{7}$$

obey the following order $w_1 > w_2 > w_3 > \cdots > w_M$ [11], where the amplitude function $A_k(t)$ and the phase function $\phi_k(t)$ can be obtained from the analytic signal of kth intrinsic mode:

$$\psi_k(t) = C_k(t) + iC_k'(t) = A_k(t)e^{i\phi_k(t)} \tag{8}$$

for $k = 1, 2, \ldots, M$, where M is the number of intrinsic modes. Correspondingly, a proper rotation for kth intrinsic mode can be

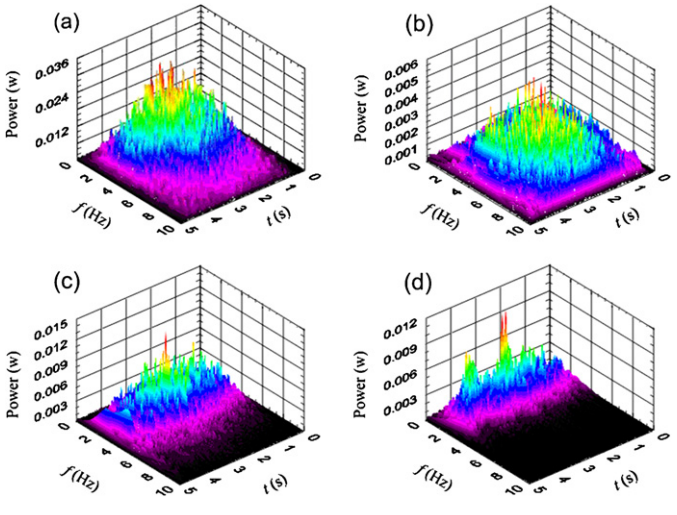

Fig. 3. (Color online.) WVD results of bubble flow ($U_{sw} = 0.18$ m/s, $U_{sg} = 0.01$ m/s) for (a) original signal; (b) 1st intrinsic mode; (c) 2nd intrinsic mode; (d) 3rd intrinsic mode. As can be seen, the frequency of original signal focuses on 1 Hz ∼ 6 Hz; the 1st intrinsic mode possesses wider and higher frequency distribution (over 10 Hz) resulting from the dynamical and/or observational noise in an experimental setting; the frequency of the 2nd intrinsic mode ranges from 1 Hz to 6 Hz within the proper range; the frequency distribution of 3rd intrinsic mode becomes much narrower and lower than that of the original signal.

obtained by plotting $C'_k(t)$ against $C_k(t)$ in the complex plane of $\psi_k(t)$. As shown in Fig. 2, the average frequencies of the rotations (the slopes) associated with various modes are distinct. The fluctuations of the phase function can then be obtained as [14]

$$\Delta\phi_k(t) = \phi_k(t) - w_k(t)t \tag{9}$$

The first mode has the highest frequency, which usually corresponds to noise. We have examined that the second intrinsic mode contains most relevant information about the original signals because its frequency obtained by using the Wigner–Ville distribution [16,17] is in good agreement with that of the original signals, as shown in Fig. 3. We thus focus on the second mode for further analysis.

After obtaining the phase fluctuations, we use the DFA method [12] to uncover the dynamical characteristics associated with long-range correlation and diffusive. The procedure begins with a time series $X(t)$ of length N. First, we calculate the accumulated series

$$C(t) = \sum_{i=1}^{t} \big(X(i) - \langle X\rangle\big) \tag{10}$$

where $\langle X\rangle = (1/N)\sum_{t=1}^{N} X(t)$. Second, we divide $C(t)$ into N_b non-overlapping boxes of equal sizes L. In each box, the local trend $C^m_{fit}(t) = at + b$ is defined to be the ordinate of a linear least-square fit of the data point in that box, where the index m indicates the box number. The detrended fluctuation $F(L)$ is then calculated following:

$$F(L) = \left(\frac{1}{N_b}\sum_{m=1}^{N_b}\frac{1}{L}\sum_{t=(m-1)L+1}^{mL}\big(C(t) - C^m_{fit}(t)\big)^2\right)^{1/2} \tag{11}$$

This function measures the root mean squared fluctuations. If $F(L)$ vs. L exhibits linear relationship on the log–log graph, it indicates the presence of scaling behavior

$$F(L) \sim L^{\alpha} \tag{12}$$

where α is the DFA scaling exponent and it depends on the correlation properties of the signal. Especially, the value of α marks

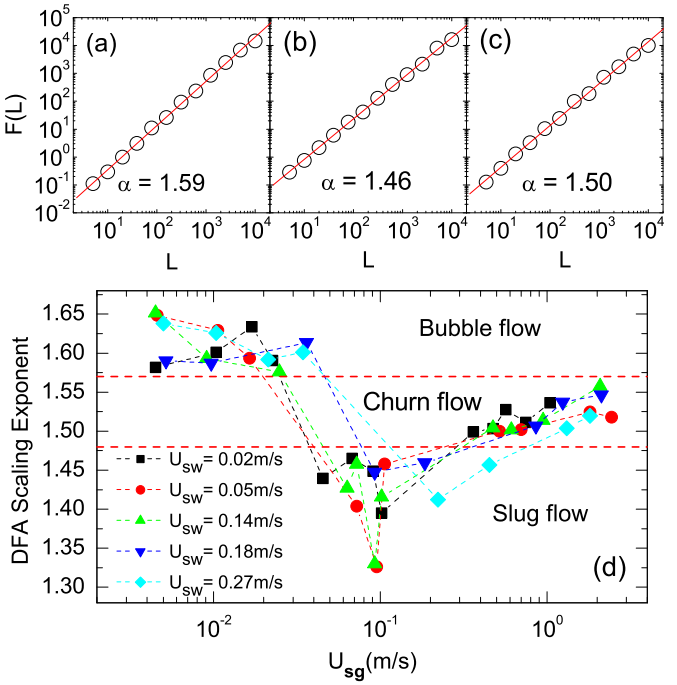

Fig. 4. (Color online.) DFA analysis of phase fluctuations of the second intrinsic mode for three typical flow patterns: (a) bubble flow ($U_{sw} = 0.18$ m/s, $U_{sg} = 0.01$ m/s); (b) slug flow ($U_{sw} = 0.18$ m/s, $U_{sg} = 0.12$ m/s); (c) churn flow ($U_{sw} = 0.18$ m/s, $U_{sg} = 0.61$ m/s). (d) DFA scaling exponent distribution on semi-log scale of 50 phase fluctuations belonging to three patterns with increase of the gas superficial velocity.

the borderline between stationary and non-stationary behavior: for $\alpha \geqslant 1$, one has non-stationary signals associated with sub-diffusive ($\alpha < 3/2$), diffusive ($\alpha = 3/2$) or super diffusive ($\alpha > 3/2$) behavior. Fig. 4 shows the scaling $F(L) \sim L^{\alpha}$ for three flow patterns from 50 experimental measurements. We see that the phase fluctuations of bubble, slug and churn flows display super-diffusive, sub-diffusive and Brownian-motion type of behaviors, respectively, in the sense that the DFA scaling exponent for bubble, slug and churn flow is 1.61 ± 0.02, 1.42 ± 0.04 and 1.51 ± 0.02 (near 1.50), respectively. Moreover, there appear to be phase transitions among three flow patterns as the gas superficial velocity U_{sg} is increased. We also note that the scaling exponent α shows a non-monotonous behavior in the transition from bubble flow to churn flow, indicating the dynamical complexity associated with two-phase flows.

Fig. 4 demonstrates that the DFA scaling exponents based on phase fluctuations for three typical types of two-phase flow patterns are located in three distinct regions without any overlap. Note that there exists an abrupt transition of DFA exponent between bubble and slug flow, indicating that the dynamical features of the two flow patterns are quite different, consistent with existent knowledge about the phase flows. These results demonstrate that our phase-fluctuation based approach is capable of characterizing and distinguishing the three typical flow patterns, especially bubble flow from churn flow, a task that existing methods based on complexity measures fail to work [18]. In the study of two-phase flow, the numerical simulation of pressure drop (or void) and the correlations closely correlate with the flow pattern. Moreover, the established flow model will vary with respect to distinct flow patterns. Thus, characterizing the system dynamical characteristics and further accurately identifying different flow patterns will provide fundamental information for the study of inherent void and pressure drop, e.g., the choose of the model for calculating the inherent void or pressure drop. For a large class of signals measured from two-phase flow system, our method can extract the

scaling exponents associated with dynamical characteristics and further identify flow patterns in a fast and visual way.

In summary, we have proposed a novel approach based on phase fluctuations and demonstrated its power to characterize and distinguish typical patterns arising from gas–liquid two-phase flow experiments. Technically our method contains two components: EMD and DFA, the former being necessary for extracting proper rotations and the latter for detection of robust scaling behavior in the phase fluctuations. Due to the generality of the method, we expect it to be useful for broader applications beyond multi-phase flows.

Acknowledgements

ZKG and NDJ were supported by NNSFC (Grant No. 50974095) and NHTRDPC (Grant No. 2007AA06Z231). WXW and YCL were supported by AFOSR under Grant No. FA9550-09-1-0260.

References

[1] S.Z. Rouhani, M.S. Sohal, Progr. Nucl. Energ. 11 (1983) 219.
[2] R.K. Das, S. Pattanayak, Meas. Sci. Technol. 4 (1993) 1457.
[3] M.G. Hubbard, A.E. Dukler, Characterization of flow regimes for horizontal two-phase flow, in: Proceedings of the 1966 Heat Transfer and Fluid Mechanics Institute, Stanford University Press, Stanford, CA, 1966.
[4] O.C. Jones, N. Zuber, Int. J. Multiphase Flow 2 (1975) 273.
[5] M.A. Vince, R.T. Lahey Jr., Int. J. Multiphase Flow 8 (1982) 93.
[6] H. Kantz, T. Schreiber, Nonlinear Time Series Analysis, Cambridge University Press, UK, 1997.
[7] C.S. Daw, W.F. Lawkins, D.J. Downing, N.E. Clapp Jr., Phys. Rev. A 41 (1990) 1179.
[8] W.F. Lawkins, C.S. Daw, D.J. Downing, N.E. Clapp Jr., Phys. Rev. E 47 (1993) 2520.
[9] C.S. Daw, C.E.A. Finney, M. Vasudevan, N.A. vanGoor, K. Nguyen, D.D. Bruns, E.J. Kostelich, C. Grebogi, E. Ott, J.A. Yorke, Phys. Rev. Lett. 75 (1995) 2308.
[10] R. Femat, J.A. Ramírez, A. Soria, Phys. Lett. A 248 (1998) 67.
[11] N.E. Huang, Z. Shen, S.R. Long, M.C. Wu, H.H. Shih, Q. Zheng, N.C. Yen, C.C. Tung, H.H. Liu, Proc. R. Soc. London A 454 (1998) 903.
[12] C.-K. Peng, S.V. Buldyrev, S. Havlin, M. Simons, H.E. Stanley, A.L. Goldberger, Phys. Rev. E 49 (1994) 1685.
[13] N.D. Jin, Z. Xin, J. Wang, Z.Y. Wang, X.H. Jia, C.P. Chen, Meas. Sci. Technol. 19 (2008) 045403.
[14] T. Yalcinkaya, Y.-C. Lai, Phys. Rev. Lett. 79 (1997) 3885.
[15] W.-S. Lam, W. Ray, P.N. Guzdar, R. Roy, Phys. Rev. Lett. 94 (2005) 010602.
[16] E. Wigner, Phys. Rev. 40 (1932) 749.
[17] J. Ville, Cable et Transmission 2A (1) (1948) 611.
[18] Z.K. Gao, N.D. Jin, Phys. Rev. E 79 (2009) 066303.